WILEY-VCH

RESEARCH ARTICLE

Controlled Supramolecular Assemblies of Chiral Cyclometalated Gold (III) Amphiphiles in Aqueous Media

Aries Kwok-Heung Chan,[a],[b],+ Ming-Hin Chau,[a],+ Yikun Ren,[a] Jia-Jun Jiang,[a] Man-Kin Wong, [a],[b],* and Franco King-Chi Leung[a],*

[a] Mr. A. K.-H. Chan, Mr. M.-H. Chau, Ms. Y. Ren, Dr. J.-J. Jiang, Prof. Dr. M.-K. Wong, Prof. Dr. F. K.-C. Leung
State Key Laboratory of Chemical Biology and Drug Discovery, Department of Applied Biology and Chemical Technology, The Hong Kong Polytechnic University, Hong Kong, China.
[b] Mr. A. K.-H. Chan, Prof. Dr. M.-K. Wong
Research Institute for Future Food, Department of Food Science and Nutrition, The Hong Kong Polytechnic University, Hong Kong, China.

E-mail: mankin.wong@polyu.edu.hk (M.-K. Wong), kingchifranco.leung@polyu.edu.hk (F.K.-C. Leung)
+These authors contributed equally to this work.

Supporting information for this article is given via a link at the end of the document.

Abstract: Gold (III) cyclometalated based amphiphiles in aqueous media have been revealed with excellent supramolecular transformations to external stimuli to open new pathways for soft functional material fabrications. Herein, we report a new chiral cyclometalated gold (III) amphiphile (**GA)** assembling into lamellar nanostructures in aqueous media confirmed with transmission electron microscopy (TEM). Counterion exchange with *D*-, *L*-, or racemic-camphorsulfonates features the significant supramolecular helicity enhancements, enabling transformations of **GA** from lamellar structure to vesicles and to nanotubes with multi-equivalents of counterion. The limited cytotoxicity of **GA** in aqueous media exhibits good biocompatibility.

Introduction

Supramolecular assemblies in nature are serving vital roles in various biological proper functions.[1–3] Advanced synthetic methodologies enable fabrications of artificial supramolecular assemblies, featured with high structural versatility and responsiveness to external stimulations,[4–7] including light, pH, ion strength, organic molecules, and organic solvents.[8–10] Amphiphilic molecular design is commonly combing both hydrophilic and hydrophobic moieties to exert good aqueous solubility and functions turnability.[4,11] Extensive developments of organic amphiphiles in aqueous media have been demonstrated with excellent examples, *e.g.*, amino acid-based, photoresponsive molecular,[4,12] and chromophore-based amphiphiles.[13–16] Chiral organic amphiphiles are ready to assemblies non-covalently into supramolecular chiral hierarchical structures, enabling additional stimulation responsiveness than that of natural counterparts.[17–19] Metal-ligand amphiphiles are the most promising alternative strategies to organic amphiphiles, in considering the diversity of metal-ligand structures and versatility of ligand designs.[20–24] Supramolecular interactions and hierarchical structures of metal-ligands amphiphiles can be systematically controlled with subtle synthetic design.[20,24]

Gold complexes have been intensively investigated for applications in catalysis,[25–29] optoelectronic materials,[30,31] and Bioconjugation strategies,[32–37] due to the excellent aqueous stability. Amphiphilic designs of gold (III) complexes were firstly reported by Che in 2016,[38] to use polyethene glycol (PEG) based cyclometalated gold (III) complexes for formation nano-micelles enabling *in-vitro* phototoxicity. Cyclometalated gold (III) amphiphiles in ACN/water media self-assembled supramolecularly with kinetic controls,[39] reported by the same group. Charged cyclometalated gold (III) amphiphiles showed multiple stimulation responsiveness and gel-sol processes in organic media,[40] reported by Yam. These reported cyclometalated gold (III) amphiphiles are highly sensitive to subtle molecular change and resulting supramolecular nanostructures.[38–40] We reported firstly the reversibly counterion controlled supramolecular transformations of cyclometalated gold (III) amphiphiles in aqueous media.[41] In comparing to well-developed organic amphiphiles, chiral supramolecular assembly of gold (III) amphiphile systems remain unexplored.

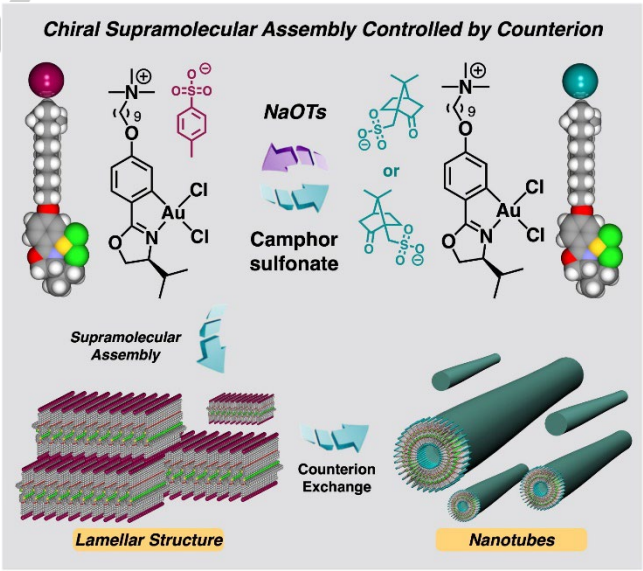

Scheme 1. Schematic illustration of the design of cyclometalated gold (III) amphiphiles. Counterion exchange enables reversible transformation of the supramolecular nanostructures.

Oxazoline-based chiral cyclometalated gold (III) complexes have been demonstrated with excellent chirality transfer in asymmetric

catalytic processes,[28] reported by Wong. In considering the distinctive chirality transfer of oxazoline-based gold (III) complex, herein, we design and synthesize a new chiral cyclometalated gold (III) amphiphile (GA) assembling in aqueous media with enhanced biocompatibility. Oxazoline-based cyclometalated gold (III) complex core is connected to a quaternary ammonium ion with an alkyl-linker, enabling improved aqueous solubility. The point chirality motif can transfer the chirality to the resulting nanostructures. Supramolecular assembly and helicity of GA can be fine-tuned with counterion exchange, including tosylate, *D*-, *L*-, or racemic-camphorsulfonates. Cytocompatibility of GA in aqueous media is shown with limited cytotoxicity. Through the investigations of the supramolecular assembling processes, counterion effect, and cytocompatibility of GA, it could enable bright prospects for fabrication of counterion controlled supramolecular soft functional materials.

Results and Discussion

Design and Synthesis of GA

GA was designed with an oxazoline-based chiral cyclometalated gold (III) complex core and functionalized with a quaternary ammonium ion moiety connected by a nonyl-linker (Scheme 1). The synthetic scheme for **GA** is shown in Scheme 2. **GA** was synthesized using 2-bromo-4-hydroxybenzaldehyde as starting material which then connected to *tert*-butyldimethylsilyl ether group with a nonyl-linker, affording compound **2**. Chiral oxazoline ligand **3** was obtained by reacting with chiral amino alcohol. Based on the reported transmetalation methodologies, gold (III) complex **7** was synthesized. The nucleophilic substitution of compound **7** with trimethylamine provided the gold (III) amphiphile **GA**. The chemical structures of newly synthesized **GA** precursors and **GA** were characterized unambiguously by ^{1}H, ^{13}C NMR, and high-resolution mass spectrometry (Figures S14–S27).

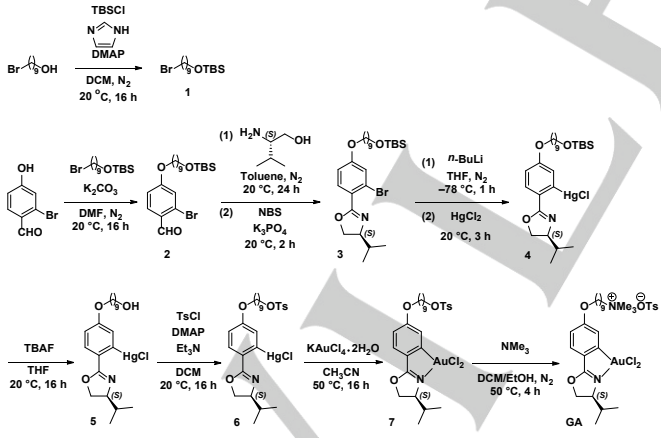

Scheme 2. Synthetic route of gold (III) amphiphiles **GA**.

Aqueous Supramolecular Assembly and Cytocompatibility of GA

A freshly prepared dichloromethane/methanol (3:1, DCM/MeOH) solution of **GA** (400 μM) showed strong absorption band at 300 nm along with shoulder band at 350 nm – 430 nm (Figure S1a). A freshly prepared aqueous solution of **GA** (12.1 mM, 1.0 weight% (wt.%)) was heated to 50 °C and slowly cooled down to 20 °C at a rate of 1.0 °C/min as the thermal annealing process. The aqueous solution of **GA** was diluted into a range of concentrations from 0.01 to 1.0 mM in determining the critical aggregation concentration (CAC) in using of dynamic light scattering measurements (DLS). The CAC of **GA** was confirmed as 80 μM (Figure S1b), indicating that the **GA** is highly soluble and form supramolecular assemblies in aqueous media. An aqueous solution of **GA** (400 μM) was heated to 50 °C and slowly cooled to 20 °C at a rate of 1.0 °C/min and subsequently studied with UV-vis absorption spectroscopy (Figure 1a). Essentially identical spectrum was observed in aqueous solution of **GA** (Figure 1a, black-line) to that of DCM/MeOH solution of **GA** (Figure S1a). It is noted that the absorbance of the absorption shoulder band at 350 nm – 430 nm decreased over the thermal annealing process with a slight hypsochromic-shift of the shoulder band (Figure 1a, red-line). The thermal annealed aqueous solution of **GA** (400 μM) was analyzed by circular dichroic (CD) measurements (Figure 1b), in showing a positive Cotton effect at 250 nm – 370 nm along with a strong negative Cotton effect at 210 nm – 250 nm. In addition, a DCM/MeOH solution of **GA** (400 μM) showed lower intensity Cotton effects (Figure S1c) than that of its aqueous solution (Figure 1b), possibly indicating supramolecular helicity generated upon dissolution in aqueous media.

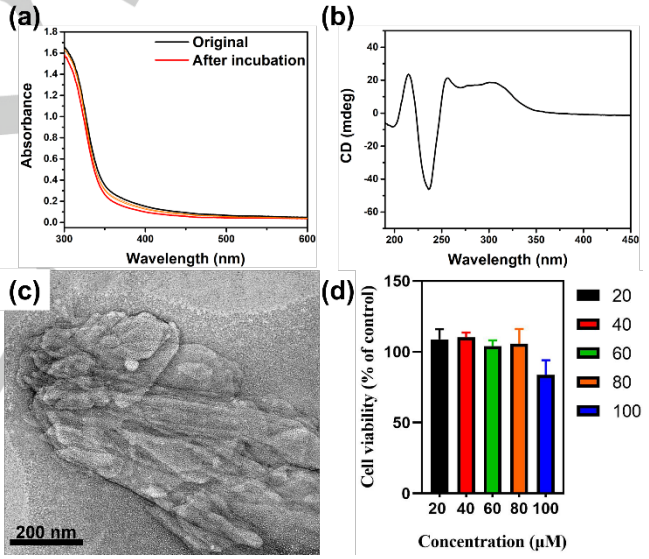

Figure 1. (a) UV-vis absorption spectra of **GA** (400 μM) in DI water before (black-line) and after incubation (red-line). (b) CD spectra of **GA** (400 μM) in DI water. (c) TEM image of thermal annealed solution of **GA** (2.42 mM). (d) hBM-MSCs viability after incubated with **GA** gradient solutions for 24 h. All values are representing as mean ± standard deviation of n = 3. * denotes *P* < 0.05, which represents for statistically difference compared to the control group.

A thermally annealed aqueous solution of **GA** (2.42 mM, 0.2 wt.%) was imaged with negative-stained transmission electron microscopy (TEM) to reveal lamellar nanostructures with irregular shape and size (width ranged from 200 nm to 1500 nm) (Figure 1c). The measured average zeta potential of thermal annealed solution of **GA** is +48.2 mV (Figure S1d), suggesting that the surface of the assembled structure is positively charged. The thermally annealed aqueous solution of **GA** was diluted and subjected for cytocompatibility studies. A MTS mitochondrial

activity assay was used for determining cell viability of human bone marrow-derived mesenchymal stem cells (hBM-MSCs) in the presence of aqueous solution of **GA** in concentration range of 20 μM – 100 μM (Figure 1d). MTS assay results were normalized to viability of hBM-MSCs in the absence of **GA**. High cell viabilities (over 90%) of hBM-MSCs over 24 h of culture with the solution of **GA** in concentration range of 20 μM – 80 μM. A subtle drop (over 80 %) of cell viability was observed in the presence of 100 μM of **GA** (Figure 1d, blue-bar). The results indicated good cytocompatibility of **GA** to hBM-MSCs cell line.

Counterion Controlled Chiral Supramolecular Assembly Transformations of GA

A thermally annealed aqueous solution of **GA** (400 μM) was added with an aqueous solution of sodium *D*-camphorsulfonate (2.0 equiv., **GA**$_{D\text{-Camphor}}$), which is originated from a common natural chiral compound camphor, and subsequently heated to 50 °C and slowly cooled to 20 °C at a rate of 1.0 °C/min. The absorption spectrum of the obtained solution shown with absorption maximum at 300 nm was reduced (Figure S2a). In using of the identical preparation method of **GA** (400 μM) with *L*-camphorsulfonate (2.0 equiv., **GA**$_{L\text{-Camphor}}$), essentially identical absorption spectra were observed (Figure S2b). With this sequential annealing preparative process of **GA** with camphorsulfonates, the obtained solutions were analyzed with CD measurements. The CD spectrum of a solution of **GA**$_{D\text{-Camphor}}$ shows stronger Cotton effect at 230 nm – 250 nm along with a weaker Cotton effect at 210 nm – 225 nm (Figure 2a, black-line) than that of **GA** solely (Figure 1b). It is noted that only limited CD signal was observed for an aqueous solution of sodium *D*-camphorsulfonate (400 μM, Figure 2a, red-line). The results clearly indicated that the chirality of counterion can transfer to GA and subsequently induce supramolecular helicity transformation. Consistently, the CD spectrum of solution of **GA**$_{L\text{-Camphor}}$ shows stronger Cotton effect at 230 nm – 250 nm along with a weaker Cotton effect at 210 nm – 225 nm (Figure 2b, black-line) than that of **GA** solely (Figure 1b). Similarly, very weak CD signal was observed for an aqueous solution of sodium *L*-camphorsulfonate (400 μM, Figure 2d, red-line). The spectral difference between **GA**$_{D\text{-Camphor}}$ and **GA**$_{L\text{-Camphor}}$ at 280 nm – 320 nm should be originated from the chirality difference between sodium *D*-camphorsulfonate and sodium *L*-camphorsulfonate. **GA** (3.86 mM, 0.2 wt.%) with *D*-camphorsulfonate (2.0 equiv.), prepared from the sequential annealing preparative process, was imaged with TEM, in showing supramolecular vesicles with a diameter range (~50 nm – 500 nm, Figures 2c and S3). While **GA** (3.86 mM, 0.2 wt.%) with *L*-camphorsulfonate (2.0 equiv.) prepared from the identical method was revealed similar supramolecular vesicle nanostructures (Figures 2d and S4). The TEM and CD results indicated the supramolecular transformations from lamellar nanostructures to supramolecular vesicles upon camphorsulfonates addition with thermal annealing. However, in consideration of the similar binding affinities of tosylate and camphorsulfonate to tetra-substituted ammonium ion of **GA**, higher ratio of camphorsulfonate should be added to substitute tosylate completely in the resulting supramolecular nanostructures.

Counterion Ratio Influence on Chiral Supramolecular Assembly Transformations of GA

A thermally annealed aqueous solution of **GA** (400 μM) was added with different ratio of aqueous solution of sodium *D*-camphorsulfonate (4.0, 6.0, 8.0, and 10.0 equiv.), and subsequently heated to 50 °C and slowly cooled to 20 °C at a rate of 1.0 °C/min. The positive Cotton effect at 230 nm – 250 nm and negative Cotton effect at 210 nm – 240 nm were increased with higher addition ratio of *D*-camphorsulfonate, observed in CD studies (Figure 3a). **GA** (3.22 mM, 0.2 wt.%) with *D*-camphorsulfonate (4.0 equiv.) prepared from the sequential annealing preparative process was imaged with TEM, in showing supramolecular vesicles along with some large aspect ratio nanostructures (Figures 3b and S5). Furthermore, the annealed solution of **GA** with *D*-camphorsulfonate (8.0 equiv.) was revealed with large aspect ratio supramolecular nanotubular structures with outer diameter (~50 nm – 200 nm, Figures 3c and S6). Though nanotubes were aggregated with vesicles upon addition of 10.0 equiv. of *D*-camphorsulfonate (Figure S7), implying that higher ratio of *D*-camphorsulfonate induce further supramolecular structural transformations with the enhanced supramolecular helicity.

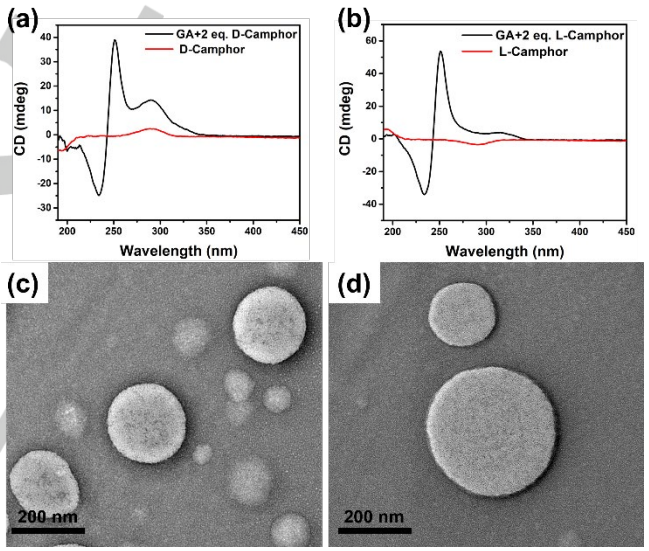

Figure 2. CD spectra of **GA** (400 μM) in DI water after addition of 2.0 equiv. of (a) sodium *D*-camphorsulfonate and (b) sodium *L*-camphorsulfonate. TEM images of a thermal annealed solution of **GA** (3.86 mM) after addition of 2.0 equiv. of (c) sodium *D*-camphorsulfonate and (d) sodium *L*-camphorsulfonate.

Furthermore, the thermally annealed aqueous solution of **GA** (400 μM) was added with different ratio of aqueous solution of sodium *L*-camphorsulfonate (4.0, 6.0, 8.0, and 10.0 equiv.), and annealed with identical method to above. In CD studies of **GA**$_{L\text{-Camphor}}$ (Figure 3d), the observed spectral shifts are essentially identical to that of observed in **GA**$_{D\text{-Camphor}}$ (Figure 3a). Both the positive Cotton effect at 230 nm – 250 nm and negative Cotton effect at 210 nm – 240 nm were increased with higher addition ratio of *L*-camphorsulfonate, observed in CD studies (Figure 3d). Upon addition of 4.0 equiv. of *L*-camphorsulfonate into annealed solution of **GA** the vesicles were transformed partially into large aspect ratio of nanofiber-like structures (Figure 3e and S8). The thermally annealed **GA**$_{L\text{-Camphor}}$ solution (8.0 equiv.) was imaged with TEM to show supramolecular nanotubes with outer diameter

range of 50 nm – 250 nm (Figure 3f and S9). Nanotubes were partially disintegrated upon addition of 10.0 equiv. of *L*-camphorsulfonate into annealed solution of **GA** (Figure S10). The TEM and CD results were revealed very similar supramolecular structure transformations and CD spectral shifts in both addition of *D*- or *L*-camphorsulfonates to **GA**, possibly indicating that the intrinsic chirality of *D*- or *L*-camphorsulfonates were not transferring to the resulting supramolecular nanostructures. In this connection, racemic mixture of camphorsulfonate (8.0 equiv.) was added to an aqueous solution of **GA** (400 μM) and treaded with the thermal annealing process. The obtained solution shows positive Cotton effect at 230 nm – 250 nm and negative Cotton effect at 210 nm – 240 nm were increased in CD studies, indicating that the counterion chirality is not transferring to the nanostructures (Figure 4a). Furthermore, the TEM image of the solution was imaged to show supramolecular nanotubes (Figures 4b and S11), which are essentially identical to that of observed in chiral- camphorsulfonates (Figure 3c and 3f). The enhancement of supramolecular helicity is possibly due to the reduced packing parameter (*P*) of **GA** from *P* = 1 to ½ < *P* <1, upon counterion addition.

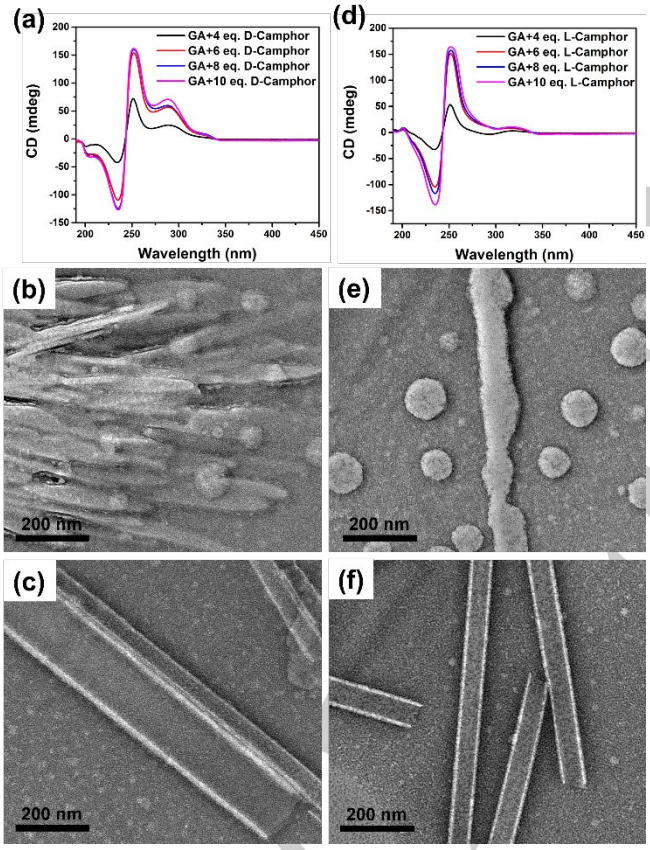

Figure 3. CD spectra of **GA** (400 μM) in DI water after addition of (a) sodium *D*-camphorsulfonate (4.0, 6.0, 8.0, and 10.0 equiv.) and (d) sodium *L*-camphorsulfonate (4.0, 6.0, 8.0, and 10.0 equiv.). TEM images of a thermal annealed solution of **GA** (3.22 mM) after addition of 4.0 equiv. of (b) sodium *D*-camphorsulfonate and (e) sodium *L*-camphorsulfonate. TEM images of a thermal annealed solution of **GA** (2.46 mM) after addition of 8.0 equiv. of (c) sodium *D*-camphorsulfonate and (f) sodium *L*-camphorsulfonate.

In considering the significant influence of counterions to the supramolecular assembly transformations and supramolecular helicity enhancements, the reversibility of these intrinsic properties of **GA** nanostructures was examined. **GA**$_{D\text{-Camphor}}$ (400 μM, 2.0 equiv. of sodium *D*-camphorsulfonate) was added sodium tosylate (2.0 equiv.) and further thermally annealed, affording lamellar structures and nanosheet-like structures in TEM (Figures 4c and S12). The images revealed that the reverse supramolecular transformation from vesicles to lamellar structures is partially feasible, though excess amount of *D*-camphorsulfonate induces complexities and competitive pathways in the supramolecular transformation processes, in affording nanosheet-like structures and enhanced supramolecular helicity (Figure 4d). Similar supramolecular transformation and helicity enhancement were observed in **GA**$_{L\text{-Camphor}}$ solution (Figure S13).

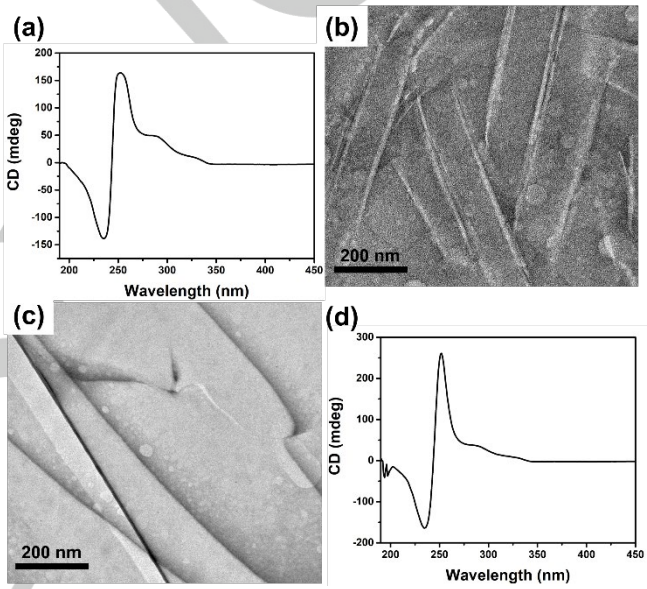

Figure 4. (a) CD spectra of **GA** (400 μM) in DI water and (b) TEM image of a thermal annealed solution of **GA** (2.46 mM) after addition of 8.0 equiv. of racemic mixture of camphorsulfonate. (c) TEM image of a thermal annealed solution of **GA**$_{D\text{-Camphor}}$ (3.26 mM) and (d) CD spectra of **GA**$_{D\text{-Camphor}}$ (400 μM) in DI water after addition of 2.0 equiv. of sodium tosylate.

Conclusion

Chiral gold (III) amphiphile was firstly designed and synthesized to show enhanced supramolecular helicities in aqueous media. Lamellar nanostructures of **GA** were confirmed with TEM. Upon addition of *D*-, *L*-, or racemic-camphorsulfonates, the counterion exchanges enable supramolecular assembly transformations from lamellar structure to vesicles, and to nanotubes with significant supramolecular helicity enhancements, though multi-equivalents of counterion is needed. The reversibility of supramolecular transformation was partially possible in the current gold (III) amphiphilic design with good cytocompatibility. The current approach is serving as the foundation to our next works on controls of supramolecular *P*-, *M*-helicities of chiral gold (III) amphiphiles with chiral counterions.

Experimental Section

Materials: All commercial reagents are purchased from Acros Organics, Sigma Aldrich, Aladdin, Macklin and Tokyo Chemical Industry Co. Ltd, and were used as received unless otherwise specified. All reactions were performed under nitrogen unless otherwise specified. Analytical thin layer chromatography (TLC) was performed with Macherey-Nagel Silica gel 60 UV254 aluminium plates and visualization was accomplished by UV light (254 / 365 nnm) or staining with phosphomolybdic acid followed by heating. Flash column chromatography was performed using Macherey-Nagel Silica gel 60 (230–400 mesh). Deuterated solvents were purchased from Cambridge Isotope Laboratories Inc. Compound **1** was synthesized and identified with reference to the characterization data of literature.[42,43]

Compound 1: To a mixture of 9-bromo-1-nonanol (4.46 g, 20 mmol), imidazole (2.72 g, 40 mmol) and 4-dimethylaminopyridine (DMAP, 244 mg, 2 mmol) under N_2, anhydrous dichloromethane (80 mL) was added. *tert*-Butyldimethylsilyl chloride (TBSCl, 3.92 g, 26 mmol) was dissolved in dichloromethane (20 mL) and added dropwise to the mixture solution. The reaction mixture was stirred at 20 °C for 16 h. When the reaction completed, the mixture solution was filtered, concentrated under vacuum and then subjected to column chromatography (hexane/ethyl acetate 30/1, R_f = 0.3) to afford compound **1** as a colorless oil (6.07 g, 18.0 mmol, 90% yield).

Compound 2: To a mixture of 2-Bromo-4-hydroxybenaldehyde (1.0 g, 5.0 mmol), compound **1** (2.0 g, 6.0 mmol) and potassium carbonate (K_2CO_3, 1.4 g, 10 mmol) under N_2, anhydrous dimethylformamide (10 mL) and was added. The reaction mixture was stirred at 20 °C for 16 h. When the reaction completed, the resulting mixture was diluted by ethyl acetate (40 mL), washed by DI water (80 mL) for three times, and dried with anhydrous $MgSO_4$. Resulting organic phase was concentrated under vacuum and subjected to column chromatography (hexane/ethyl acetate 30/1, R_f = 0.3), affording compound **2** as a pale-yellow oil (2.26 g, 4.95 mmol, 99% yield). ^{1}H NMR (400 MHz, Chloroform-*d*) δ 10.21 (s, 1H), 7.87 (d, J8.7 Hz, 1H), 7.12 (d, *J* = 2.4 Hz, 1H), 6.91 (dd, *J* = 8.4, 1.8 Hz, 1H), 4.01 (t, *J* = 6.5 Hz, 2H), 3.59 (t, *J* = 6.6 Hz, 2H), 1.84 – 1.74 (m, 2H), 1.50 (d, *J* = 6.7 Hz, 2H), 1.44 (q, *J* = 7.0 Hz, 2H), 1.31 (s, 8H), 0.89 (s, 9H), 0.04 (s, 6H). ^{13}C NMR (101 MHz, Chloroform-*d*) δ 190.65, 164.22, 131.33, 128.78, 126.76, 118.97, 114.51, 68.83, 63.30, 32.86, 29.50, 29.35, 29.23, 28.93, 26.00, 25.88, 25.78, 18.39, -5.24. HRMS (ESI): calculated for $C_{22}H_{37}BrO_3Si$ [M+H] 457.1768, found 457.1769.

Compound 3: To a mixture of compound **2** (1.0 g, 2.2 mmol) and (*S*)-valinol (225 mg, 2.19 mmol) under N_2, toluene (5 mL) was added. The mixture solution was stirred in 20 °C for 24 h, followed by addition of potassium phosphate (K_3PO_4, 1.4 g, 6.6 mmol) and *N*-Bromosuccinimide (NBS, 390 mg, 2.2 mmol). The reaction mixture was stirred at 20 °C for further 2 h. When the reaction completed, the resulting mixture solution was washed by saturated $NaHCO_3$ aqueous solution (5 mL) and saturated $Na_2S_2O_3$ solution (5 mL). Resulting organic phase was dried with anhydrous $MgSO_4$, concentrated under vacuum and subjected to column chromatography (hexane/ethyl acetate 10/1, R_f = 0.3) to afford compound **3** as a colorless oil (549 mg, 1.0 mmol, 46% yield). ^{1}H NMR (600 MHz, Chloroform-*d*) δ 7.63 (d, *J* = 8.7 Hz, 1H), 7.15 (d, *J* = 2.5 Hz, 1H), 6.83 (dd, *J* = 8.7, 2.4 Hz, 1H), 4.42 – 4.36 (m, 1H), 4.17 – 4.09 (m, 2H), 3.95 (t, *J* = 6.6 Hz, 2H), 3.59 (t, *J* = 6.7 Hz, 2H), 1.93 – 1.83 (m, 1H), 1.76 (p, *J* = 6.8 Hz, 2H), 1.51 (p, *J* = 6.8 Hz, 2H), 1.43 (p, *J* = 7.1 Hz, 2H), 1.37 – 1.28 (m, 9H), 1.04 (d, *J* = 6.8 Hz, 3H), 0.96 (d, *J* = 6.8 Hz, 3H), 0.89 (s, 9H), 0.04 (s, 6H). ^{13}C NMR (151 MHz, Chloroform-*d*) δ 162.66, 160.92, 132.33, 122.56, 121.78, 119.63, 113.51, 72.79, 70.03, 68.44, 63.32, 32.87, 32.73, 29.52, 29.36, 29.28, 29.02, 26.01, 25.92, 25.79, 18.82, 18.40, 18.18, -5.23. HRMS (ESI): calculated for $C_{27}H_{46}BrNO_3Si$ [M+H] 540.2503, found 540.2527.

Compound 4: The solution of compound **3** (521 mg, 0.96 mmol) in anhydrous THF (10 mL) was cooled to –78 °C under N_2, followed by the dropwise addition of *n*-butyllithium (2.5 M solution in hexane, 0.5 mL). The mixture solution was stirred at –78 °C for 1 h, and mercury(II) chloride ($HgCl_2$, 326 mg, 1.2 mmol) was added. The reaction mixture was then slowly warmed to 20 °C and stirred for further 3 h. When the reaction completed, saturated NH_4Cl aqueous solution (10 mL) was added. The aqueous phase was extracted by dichloromethane (20 mL × 2). The organic phase was combined, dried with anhydrous $MgSO_4$, concentrated under vacuum, and subjected to column chromatography (hexane/ethyl acetate 2/1, R_f = 0.5), affording compound **4** as a colorless oil (492 mg, 0.71 mmol, 74% yield). ^{1}H NMR (400 MHz, Chloroform-*d*) δ 7.81 (d, *J* = 8.7 Hz, 1H), 6.94 (d, *J* = 2.7 Hz, 1H), 6.80 (dd, *J* = 8.6, 2.6 Hz, 1H), 4.56 – 4.47 (m, 1H), 4.16 (t, *J* = 8.4 Hz, 1H), 4.03 – 3.92 (m, 3H), 3.60 (t, *J* = 6.6 Hz, 2H), 1.84-1.69 (m, 3H), 1.51 (t, *J* = 6.8 Hz, 2H), 1.48 – 1.40 (m, 2H), 1.31 (s, 8H), 1.05 (d, *J* = 6.7 Hz, 3H), 0.96 (d, *J* = 6.8 Hz, 3H), 0.89 (s, 9H), 0.04 (s, 6H). ^{13}C NMR (101 MHz, Chloroform-*d*) δ 167.81, 162.03, 129.70, 124.27, 123.11, 113.76, 72.46, 72.03, 68.28, 63.32, 33.10, 32.87, 29.54, 29.38, 29.32, 29.13, 26.01, 25.98, 25.80, 18.98, 18.40, -5.23. HRMS (ESI): calculated for $C_{27}H_{46}ClHgNO_3Si$ [M+H] 689.2715, found 689.2720.

Compound 5: To a solution of compound **4** (370 mg, 0.53 mmol) in THF (2 mL), tetra-*n*-butylammonium fluoride (TBAF, 1.0 M solution in THF, 0.6 mL) was added. The reaction mixture was stirred at 20 °C for 16 h, When the reaction completed, the resulting mixture was concentrated under vacuum and subjected to column chromatography (dichloromethane/ethyl acetate 20/1, R_f = 0.3), affording compound **5** as a white solid (214 mg, 0.37 mmol, 69% yield). ^{1}H NMR (600 MHz, Chloroform-*d*) δ 7.81 (d, *J* = 8.6 Hz, 1H), 6.95 (d, *J* = 2.6 Hz, 1H), 6.81 (dd, *J* = 8.6, 2.6 Hz, 1H), 4.52 (dd, *J* = 9.7, 8.4 Hz, 1H), 4.16 (t, *J* = 8.5 Hz, 1H), 4.02 – 3.94 (m, 3H), 3.64 (h, *J* = 3.6 Hz, 2H), 1.57 (p, *J* = 6.5 Hz, 2H), 1.49 – 1.41 (m, 2H), 1.39 – 1.30 (m, 8H), 1.26 (t, *J* = 5.3 Hz, 1H), 1.05 (d, *J* = 6.7 Hz, 3H), 0.96 (d, *J* = 6.9 Hz, 3H). ^{13}C NMR (151 MHz, Chloroform-*d*) δ 167.80, 162.02, 129.70, 124.30, 123.12, 113.77, 72.48, 72.03, 68.26, 63.08, 33.11, 32.78, 29.50, 29.35, 29.28, 29.10, 25.97, 25.73, 19.00, 18.98. HRMS (ESI): calculated for $C_{21}H_{32}ClHgNO_3$ [M+H] 584.1850, found 584.1846.

Compound 6: To a mixture solution of compound **5** (214 mg, 0.37 mmol) and DMAP (5 mg, 0.04 mmol), triethylamine (Et_3N, 0.2 mL) and anhydrous dichloromethane (4 mL) was added. *p*-Toluenesulfonyl chloride (TsCl, 88 mg, 0.46 mmol) was added in portion. The reaction mixture was stirred at 20 °C for 16 h. When the reaction completed, the resulting mixture was concentrated under vacuum and subjected to column chromatography (hexane/dichloromethane 1/2, R_f = 0.5), affording compound **6** as

colorless oil (206 mg, 0.28 mmol, 76% yield). ^{1}H NMR (600 MHz, Chloroform-*d*) δ 7.81 (d, *J* = 8.6 Hz, 1H), 7.78 (d, *J* = 8.4 Hz, 2H), 7.34 (d, *J* = 8.4 Hz, 2H), 6.94 (d, *J* = 2.5 Hz, 1H), 6.80 (dd, *J* = 8.6, 2.6 Hz, 1H), 4.52 (dd, *J* = 9.7, 8.3 Hz, 1H), 4.15 (t, *J* = 8.5 Hz, 1H), 4.01 (t, *J* = 6.5 Hz, 2H), 3.99 – 3.93 (m, 3H), 2.44 (s, 3H), 1.80 – 1.70 (m, 3H), 1.65 – 1.59 (m, 2H), 1.45 – 1.38 (m, 2H), 1.34 – 1.28 (m, 4H), 1.28 – 1.22 (m, 4H), 1.04 (d, *J* = 6.7 Hz, 3H), 0.95 (d, *J* = 6.7 Hz, 3H). ^{13}C NMR (151 MHz, Chloroform-*d*) δ 167.79, 161.99, 152.46, 144.67, 133.19, 129.84, 129.71, 127.90, 124.30, 123.11, 113.74, 72.49, 72.03, 70.69, 68.21, 33.11, 29.30, 29.20, 29.09, 28.87, 28.81, 25.94, 25.33, 21.68, 19.02, 18.99. HRMS (ESI): calculated for $C_{28}H_{38}ClHgNO_5S$ [M+H] 738.1938, found 738.1936.

Compound 7: To a mixture of compound **6** (135 mg, 0.14 mmol) and $KAuCl_4 \cdot 2H_2O$ (91 mg, 0.22 mmol), acetonitrile (1 mL) and was added. The reaction mixture was stirred at 50 °C for 16 h. When the reaction completed, the resulting solution was dried under reduced pressure and suspended by dichloromethane. The suspension was filtered through celite. The filtrate was subjected to column chromatography (dichloromethane, R_f = 0.5), affording to obtain crude product. The crude product was recrystallized (dichloromethane/methanol) to obtain compound **7** as white solid (111 mg, 0.144 mmol, 79% yield). ^{1}H NMR (600 MHz, Chloroform-*d*) δ 7.78 (d, *J* = 8.3 Hz, 2H), 7.33 (dd, *J* = 10.2, 8.3 Hz, 3H), 7.29 (d, *J* = 2.3 Hz, 1H), 6.78 (dd, *J* = 8.5, 2.4 Hz, 1H), 4.94 (t, *J* = 9.3 Hz, 1H), 4.83 (dd, *J* = 9.0, 4.0 Hz, 1H), 4.67 (dt, *J* = 9.5, 3.7 Hz, 1H), 4.00 (t, *J* = 6.5 Hz, 2H), 4.00 – 3.93 (m, 2H), 2.85 – 2.72 (m, 1H), 2.44 (s, 3H), 1.76 (p, *J* = 6.5 Hz, 2H), 1.67 – 1.61 (m, 2H), 1.41 (p, *J* = 7.8, 7.3 Hz, 2H), 1.35 – 1.28 (m, 4H), 1.28 – 1.20 (m, 4H), 0.96 (d, *J* = 7.0 Hz, 3H), 0.79 (d, *J* = 7.0 Hz, 3H). ^{13}C NMR (151 MHz, Chloroform-*d*) δ 180.13, 163.30, 149.58, 144.70, 133.14, 129.98, 129.85, 127.89, 116.84, 115.84, 114.82, 72.87, 70.71, 68.77, 66.57, 29.27, 29.15, 29.10, 28.90, 28.85, 28.81, 25.85, 25.33, 21.69, 18.43, 13.82. HRMS (ESI): calculated for $C_{28}H_{38}AuCl_2NO_5S$ [M-Cl] 732.1819, found 732.1815.

GA: Compound **7** (35 mg, 0.046 mmol), trimethylamine solution in ethanol (20%) (1 mL) and dichloromethane (1 mL) were mixed in a pressure tube and protected by N_2. The pressure tube was sealed and heated at 50 °C for 4 h. When the reaction completed, the mixture was dried under vacuum. The resulting residue was dissolved in dichloromethane/methanol (10/1), and was subject to column chromatography (dichloromethane/methanol), affording **GA** as white solid (12.5 mg, 0.015 mmol, 33% yield). ^{1}H NMR (600 MHz, Methanol-d_4) δ 7.71 (d, *J* = 8.2 Hz, 4H), 7.43 (d, *J* = 8.5 Hz, 1H), 7.29 (d, *J* = 2.4 Hz, 1H), 7.24 (d, *J* = 8.2 Hz, 4H), 6.93 (dd, *J* = 8.4, 2.4 Hz, 1H), 5.04 (dd, *J* = 9.3, 4.2 Hz, 1H), 4.98 (t, *J* = 9.3 Hz, 1H), 4.60 (dt, *J* = 9.4, 4.0 Hz, 1H), 4.07 (t, *J* = 6.5 Hz, 2H), 3.35 – 3.32 (m, 2H), 3.12 (s, 9H), 2.76 – 2.67 (m, 1H), 2.37 (s, 6H), 1.84 – 1.75 (m, 4H), 1.50 (p, *J* = 7.4 Hz, 2H), 1.44 – 1.36 (m, 8H), 0.98 (d, *J* = 7.1 Hz, 3H), 0.83 (d, *J* = 7.0 Hz, 3H). ^{13}C NMR (151 MHz, Methanol-d_4) δ 180.24, 163.18, 148.57, 142.07, 140.34, 130.08, 128.44, 125.56, 117.18, 116.02, 114.06, 73.05, 68.58, 66.58, 66.46, 52.11, 29.19, 28.95, 28.79, 28.72, 28.47, 25.92, 25.51, 22.56, 19.93, 16.95, 12.49. HRMS (ESI): calculated for $C_{31}H_{47}AuCl_2N_2O5_S$ [M-OTs] 655.2127, found 655.2155.

Preparation of aqueous sample: **GA** (1 wt.%) was dissolved in fresh deionized water (DI water). The solution was heated at 50 °C for 5 min, then slowly cooled to 20 °C at a rate of 1.0 °C/min to form assembled structure. For TEM study, the annealed solution was further diluted to 0.2 wt.%.

Incubation of GA with Sodium *L*-camphorsulfonate and Sodium *D*-camphorsulfonate for Counter Anion Controlled Supramolecular Transformation: A thermal annealed aqueous solution of **GA** (12.1 mM) was added with an aqueous solution of sodium *L*-camphorsulfonate or sodium *D*-camphorsulfonate (2.0, 4.0, 6.0, 8.0, and 10.0 equiv.). The obtained solution was incubated at 50 °C for 5 min, and slowly cooled down to 20 °C at a rate of 1.0 °C/min.

Circular Dichroism (CD) Spectroscopy: CD measurements were performed on a Jasco J-1500 CD spectrophotometer at room temperature. A quartz cuvette with an optical pathlength of 1.0 mm was used for the CD spectroscopy measurements.

Cytotoxicity test: The cytotoxicity of **GA** was characterized by 3-(4,5-dimethylthiazol-2-yl)-5-(3-carboxymethoxyphenyl)-2-(4-sulfophenyl)-2H-tetrazolium (MTS) assay. Human bone-marrow Mesenchymal Stem Cells (hBM-MSCs) were seeded in 96-well plate as a density of 3000 cells per well. After incubated in growth media which contains Minimum Essential Medium (MEM Alpha, no phenol red, Gibco, USA), 10% Fetal Bovine Serum (FBS, Gibco, USA) and 1% Antibiotic-Antimycotic (Gibco, USA) for 12 h, different concentration of **GA** was added and incubated with cells for 24 h, respectively. For MTS assay, MTS solution was added to each well and incubated for 2 h at 37 °C and 5% CO_2. The absorbance of each well was measured at 490 nm using LEDETECT 96 microplate reader. Human stem cells were used to demonstrate the higher application potential for biomedical materials.

Dynamic Light Scattering (DLS): Dynamic Light Scattering intensities of each sample were measured on a Wyatt Technology DynaPro NanoStar. The scattering intensities were recorded as a parameter for assembly size, given that the objects in solution are anisotropic and the models used by Wyatt software are fitting for spherical objects. The critical aggregation concentration (CAC) of **GA** is determined by the scattering intensities of the solutions of **GA** (concentration: 1.0×10^{-3} to 1.0 mM) at 20 °C. The scattering rate was normalized by the concentration of the solution to yield the molar scattering intensity (M Counts s^{-1} m^{-1}). Ten replications were performed, and the data was averaged to show the molar scattering intensity and corresponding standard deviation.

Transmission Electron Microscopy (TEM): TEM was performed on a JEOL Model JEM-2010 Transmission Electron Microscope with hair pin type tungsten filament operating at 120 kV equipped with Gatan 794 CCD camera. TEM sample was prepared by depositing sample solutions (5.0 μL) onto a carbon grid (Micro to Nano, EMR Carbon support film on copper, 400 square mesh) for 20 s. The sample solution was removed by blotting and UranyLess EM stain solution (Electron Microscopy Science, 5.0 μL) was directly deposited onto the grid for 20 s and the stain was removed by blotting.

UV-vis Spectroscopy: UV-vis measurements were performed on Agilent Cary 60 UV-visible Spectrophotometer with a 1 cm path length quartz cuvette. A Luma 40/8453 temperature-controlled cuvette holder with four optical ports was mounted in the sample

compartment of Agilent Cary 60 UV-visible Spectrophotometer. Measurement of all samples were carried out at 20 °C unless otherwise specified.

Zeta potential measurement: Zeta potential of the thermal annealed solution of **GA** (400 *μ*M) was measured with a Zetasizer Nano-ZSZEN 3600 Zetasizer (Malvern Panalytica) by using a He-Ne laser at a wavelength of 632.8 nm in a disposable folded capillary cell (Malvern Panalytica, DTS1070). Three replicates were performed and the data was averaged.

Acknowledgements

This work was supported financially by the Croucher Foundation (Croucher Innovation Award-2021), the Hong Kong Research Grant Council (GRF 15305822 to F.K.C.L.), (GRF 15300019 and 15300520 to M.K.W.), and The Hong Kong Polytechnic University (W08A, ZVST). We acknowledge the technical support from UCEA and ULS of PolyU.

Keywords: amphiphiles • chirality • gold • self-assembly • supramolecular chemistry

References

[1] N. S. Simmons, E. R. Blout, *Biophys. J.* **1960**, *1*, 55–62.
[2] T. Lino, *J. Supramol. Struct.* **1974**, *2*, 372–384.
[3] D. Chapman, *Q. Rev. Biophys.* **1975**, *8*, 185–235.
[4] S. Chen, R. Costil, F. K.-C. Leung, B. L. Feringa, *Angew. Chem. Int. Ed.* **2021**, *60*, 11604–11627.
[5] B. L. Feringa, *Angew. Chem. Int. Ed.* **2017**, *56*, 11060–11078.
[6] E. Krieg, M. M. C. Bastings, P. Besenius, B. Rybtchinski, *Chem. Rev.* **2016**, *116*, 2414–2477.
[7] T. Aida, E. W. Meijer, S. I. Stupp, *Science* **2012**, *335*, 813–817.
[8] D. Dattler, G. Fuks, J. Heiser, E. Moulin, A. Perrot, X. Yao, N. Giuseppone, *Chem. Rev.* **2020**, *120*, 310–433.
[9] M. Baroncini, S. Silvi, A. Credi, *Chem. Rev.* **2020**, *120*, 200–268.
[10] H. Shigemitsu, T. Fujisaku, W. Tanaka, R. Kubota, S. Minami, K. Urayama, I. Hamachi, *Nat. Nanotechnol.* **2018**, *13*, 165–172.
[11] J. Volarić, W. Szymanski, N. A. Simeth, B. L. Feringa, *Chem. Soc. Rev.* **2021**, *50*, 12377–12449.
[12] A. K.-H. Chau, F. K.-C. Leung, *Adv. Colloid Interface Sci.* **2023**, *315*, 102892.
[13] M.-H. Chau, M. C. A. Stuart, F. K.-C. Leung, *Colloids Surf. A* **2023**, *661*, 130939.
[14] L.-H. Cheung, T. Kajitani, F. K.-C. Leung, *J. Colloid Interface Sci.* **2022**, *628*, 984–993.
[15] A. K.-H. Chau, L.-H. Cheung, F. K.-C. Leung, *Dyes Pigm.* **2022**, *208*, 110807.
[16] K. S.-Y. Kwan, Y.-Y. Lui, T. Kajitani, F. K.-C. Leung, *Macromol. Rapid Commun.* **2022**, *43*, 2200438.
[17] M. A. Mateos-Timoneda, M. Crego-Calama, D. N. Reinhoudt, *Chem. Soc. Rev.* **2004**, *33*, 363–372.
[18] M. Liu, L. Zhang, T. Wang, *Chem. Rev.* **2015**, *115*, 7304–7397.
[19] G. Ouyang, M. Liu, *Mater. Chem. Front.* **2020**, *4*, 155–167.
[20] J. K.-L. Poon, Z. Chen, S. Y.-L. Leung, M.-Y. Leung, V. W.-W. Yam, *Proc. Natl. Acad. Sci.* **2021**, *118*, e2022829118.
[21] V. W.-W. Yam, A. S.-Y. Law, *J. Chin. Chem. Soc.* **2020**, *67*, 2246–2252.
[22] H. L.-K. Fu, V. W.-W. Yam, *Chem. Lett.* **2018**, *47*, 605–610.
[23] T. Owen, A. Butler, *Coord. Chem. Rev.* **2011**, *255*, 678–687.
[24] M. J. Mayoral Muñoz, G. Fernández, *Chem. Sci.* **2012**, *3*, 1395–1398.
[25] W. Zi, F. Dean Toste, *Chem. Soc. Rev.* **2016**, *45*, 4567–4589.
[26] J.-J. Jiang, M.-K. Wong, *Chem. Asian J.* **2021**, *16*, 364–377.
[27] L. Rocchigiani, M. Bochmann, *Chem. Rev.* **2021**, *121*, 8364–8451.
[28] J.-J. Jiang, J.-F. Cui, B. Yang, Y. Ning, N. C.-H. Lai, M.-K. Wong, *Org. Lett.* **2019**, *21*, 6289–6294.
[29] J.-F. Cui, H.-M. Ko, K.-P. Shing, J.-R. Deng, N. C.-H. Lai, M.-K. Wong, *Angew. Chem. Int. Ed.* **2017**, *56*, 3074–3079.
[30] V. W.-W. Yam, A. K.-W. Chan, E. Y.-H. Hong, *Nat. Rev. Chem.* **2020**, *4*, 528–541.
[31] V. W.-W. Yam, V. K.-M. Au, S. Y.-L. Leung, *Chem. Rev.* **2015**, *115*, 7589–7728.
[32] P. Destito, C. Vidal, F. López, J. L. Mascareñas, *Chem. Eur. J.* **2021**, *27*, 4789–4816.
[33] S. R. Thomas, A. Casini, *Curr. Opin. Chem. Biol.* **2020**, *55*, 103–110.
[34] T.-C. Chang, K. Tanaka, *Bioorg. Med. Chem.* **2021**, *46*, 116353.
[35] H.-Y. Sit, B. Yang, K. K.-Y. Kung, J. S.-L. Tam, M.-K. Wong, *Chempluschem* **2019**, *84*, 1739–1743.
[36] K. K.-Y. Kung, H.-M. Ko, J.-F. Cui, H.-C. Chong, Y.-C. Leung, M.-K. Wong, *Chem. Commun.* **2014**, *50*, 11899–11902.
[37] H.-M. Ko, J.-R. Deng, J.-F. Cui, K. K.-Y. Kung, Y.-C. Leung, M.-K. Wong, *Bioorg. Med. Chem.* **2020**, *28*, 115375.
[38] F. Wang, M. Lan, W.-P. To, K. Li, C.-N. Lok, P. Wang, C.-M. Che, *Chem. Commun.* **2016**, *52*, 13273–13276.
[39] Q. Wan, J. Xia, W. Lu, J. Yang, C.-M. Che, *J. Am. Chem. Soc.* **2019**, *141*, 11572–11582.
[40] M.-Y. Leung, S. Y.-L. Leung, K.-C. Yim, A. K.-W. Chan, M. Ng, V. W.-W. Yam, *J. Am. Chem. Soc.* **2019**, *141*, 19466–19478.
[41] J.-J. Jiang, A. K.-H. Chau, M.-K. Wong, F. K.-C. Leung, *Eur. J. Inorg. Chem.* **2022**, *2022*, e202200281.
[42] A. M. Bailey, S. Wolfrum, E. M. Carreira, *Angew. Chem. Int. Ed.* **2016**, *55*, 639–643.
[43] R. Tuladhar, N. Yarravarapu, Y. Ma, C. Zhang, J. Herbert, J. Kim, C. Chen, L. Lum, *J. Biol. Chem.* **2019**, *294*, 6273–6282.

Entry for the Table of Contents

Insert graphic for Table of Contents here.

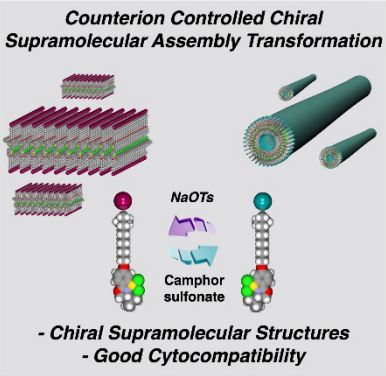

Insert text for Table of Contents here.

The first chiral gold (III) amphiphile enables chiral supramolecular assembly in aqueous media, confirmed by circular dichroic and electron microscopy, with potential supramolecular helicity enhancement controlled by packing parameters of the amphiphilic design. The resulting chiral supramolecular assembly shows good cytocompatibility.